Critical Analysis of Coefficient of Friction Derivation Methods for Fretting under Gross Slip Regime

I. Llavori[1,*], A. Zabala[1], A. Aginagalde[1], W. Tato[1], J.J. Ayerdi[1], X. Gómez[1]

[1] Surface Technologies, Mondragon University, Faculty of Engineering, Loramendi 4, 20500 Arrasate-Mondragon, Spain.

*Corresponding author: Iñigo Llavori, illavori@mondragon.edu

Abstract

This work presents a critical analysis of coefficient of friction derivation methods for fretting under gross slip regime. A mass review of tribology journals revealed that 41% of papers did not specify the derivation method used and 37% employed the least effective methods. Following an analytical and experimental study, the use of the geometric independent coefficient of friction method (GICoF) is suggested for gross slip regime due to its robustness, followed by the energy method (ECoF). This study highlights the importance of the correct selection of the coefficient of friction method and it quantifies potential errors.

Keywords: Friction, coefficient of friction, fretting loop; fretting

Nomenclature

Abbreviations

CoF	= Coefficient of friction
ECoF	= Energy coefficient of friction
GICoF	= Geometric independent coefficient of friction
max(CoF)	= Maximum coefficient of friction
mean(CoF)	= Mean coefficient of friction
FL	= Fretting loop

Symbols

E_d = Dissipated friction energy over a cycle

F_N = Normal force

F_R = Friction force

P = Contact force

Q = Tangential force

Q^* = Tangential force amplitude

S = Tangential contact stiffness

x_0 = Half-width of the wear scar

z_0 = Depth of the wear scar

δ = Slip

δ^* = Slip amplitude

$|\dot{\delta}|/\dot{\delta}$ = Direction of motion

Δ = Applied displacement

Δ^* = Applied displacement amplitude

μ = True contact CoF

μ_E = Energy coefficient of friction

1.- Introduction

Fretting occurs in a relatively small displacement (< 300 μm) between two or more contacting bodies [1]. Depending on the contact loading and relative displacement amplitude, fretting sliding can occur either in partial or gross slip conditions [2]. In the partial slip regime, relative slip between the contact bodies occurs on the edge of the contact surface. This regime promotes the nucleation of cracks and its subsequent propagation, and it generally gives rise to fretting fatigue failure [3]. When the whole contact area slips, gross sliding regime takes place, which gives rise to material removal degradation and promotes competition between crack propagation and wear [3]. Fretting fatigue and fretting wear damage have great economical and safety impact on different industries such as aerospace [4], nuclear [5], lifts [6], bio-implants [7] and railway [8]. Understanding and predicting this phenomenon is thus of great significance in determining, among others, the lifetime of safety-critical components.

Literature mentions a myriad of variables affecting fretting behaviour. Dobromirski [9] introduces a classification into (i) primary variables—which include the coefficient of friction (CoF), slip amplitude and contact pressure—and (ii) secondary variables. It should be highlighted that the CoF is pointed out as the main variable of the primary variables, and to be the scaling factor of the axial stress produced by the tangential force [10].

In spite of its significance, however, there is no agreed definition on the CoF in a fretting test [11]. CoF in the gross slip regime is extracted from the plot of tangential force Q against relative displacement Δ for each cycle of oscillation, which is commonly referred to as tangential force hysteresis loop or fretting loop (FL). The FL area is mainly defined by the actual applied displacement amplitude Δ^*, the tangential force during sliding Q and tangential contact stiffness S. The latter is used to describe the slope of the micro-slip part of the loop due to the compliance in the system, associated with elastic deformation of the specimen, the fixture, and the test rig [12]. **Fig. 1** presents a schematic of a frictional hysteresis loop observed in a gross slip fretting test, and it shows both Coulomb and the commonly observed non-Coulomb frictional behaviour.

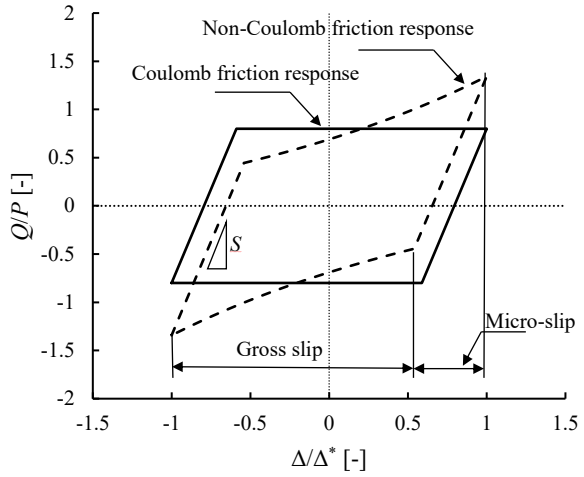

Fig. 1. Schematic illustrations of different fretting loops with the flat topped Coulomb and the hook-like non-Coulomb hysteresis loops.

The impact of the derivation method on the CoF has been proven important [11,13]. Different approaches could report significantly different CoFs, which may significantly impact the performance prediction. For example, in fretting fatigue life assessment simulation, higher CoFs predict shorter lifespan [10]. Considering the number of published studies resorting to different derivative methods, studying the scale of differences between the coefficients derived via different strategies is deemed appropriate.

This study introduces a critical analysis of coefficient of friction derivation methods for fretting under gross slip regime. To that end, first the prevalence of the derivative methods used in the published literature is analysed through a mass review of two highly regarded journals, namely, *Tribology International* and *Wear*, for the period 2009–2019. Afterwards, the most commonly used derivative methods are reviewed and the impact of the derivative method according to the fretting loop shape is subjected to virtually generated synthetic fretting loop theoretical analysis. Finally, a case study on thin steel wires demonstrates the influence of a large wear scar and its effect on the calculated CoF value.

2.- Review of the coefficient of friction derivation methods

A search was performed on the ScienceDirect website by entering the keyword "fretting". Papers on the gross slip regime published in the top two journals devoted to tribology (*Tribology International* and *Wear*) were included in the analysis. A total of 163 papers published between 2009−2019 were analysed for their applied CoF derivation method. The selected papers were examined by two assessors, and, in order to test the reliability of the results, 10% of the papers read by each assessor were reread by a third one. The detailed results of the analysis are included in the **Additional material** section. From the 163 papers selected for analysis, as many as 67 (41%) did not specify the applied method. Among the other 96 papers, four different CoF derivation methods were identified:

- Maximum value of the tangential force over a cycle (max(CoF)), 50 papers (30%);
- Mean value of the tangential force (mean(CoF)), 12 papers (7%);
- Energy coefficient of friction (ECoF), 34 papers (21%);
- Geometric independent coefficient of friction (GICoF), three papers (2%).

In what follows, the four respective CoF calculation methods are reviewed.

2.1 Maximum coefficient of friction

The max(CoF) method is defined as the ratio between the maximum value of the tangential force Q^* (or tangential force amplitude) within a cycle and the contact load P. A simple search algorithm of the type $|Q|_{max}$ or $(Q_{max} - Q_{min})/2$ within a cycle can be used to define the max(CoF) as Q^*/P. This is an effective method for ideal parallelogram-shaped loops where the tractional force does not change across the stroke according to Coulomb's friction law. However, non-Coulomb behaviour has often been reported together with an increase in the tangential force (Q) across the stroke (2Δ) [14–19]. For

frictional hysteresis loops with non-Coulomb behaviour, the use of the maximum tractional force as a representative CoF value to characterise the total loop was deemed inappropriate [11] due to the high peak loop value shown in **Fig. 2**. It is worth noting that experimental friction loops are never straight lines due to the inherent noise. Seeing that only one or two points are needed to compute the CoF with the max(CoF) method, careful filtering may be required.

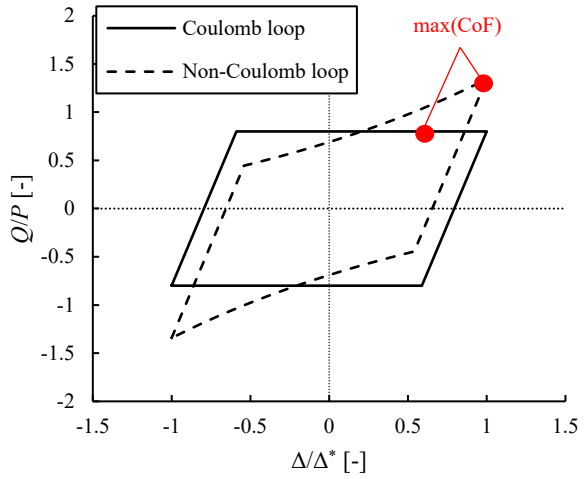

Fig. 2. Examples of Coulomb and non-Coulomb fretting loops indicating the location of max(CoF).

2.2 Mean coefficient of friction

The mean(CoF) method computes the mean absolute value of each cycle in a data set. The method therefore integrates within the time domain, since the recorded data by the sensor is usually equally spaced in a certain frequency acquisition time (**Fig. 3**). It is widely used in tribological configurations, such as pin on disc and linear reciprocating tests, where the sticking portion at the beginning and the end of the stroke is negligible compared to the sliding portion. In fretting, however, the slip range is highly sensitive to system stiffness [11], and the sticking part of the test could negatively influence the CoF calculation (**Fig. 3**). On the other hand, in cases exhibiting non-Coulomb behaviour, the hook-like feature (i.e. the increase of the tangential force in the sliding portion) occurs when the velocity is lowest. Consequently, the accumulated data is very high near the max(CoF) point and could thus lead to overestimating the CoF value.

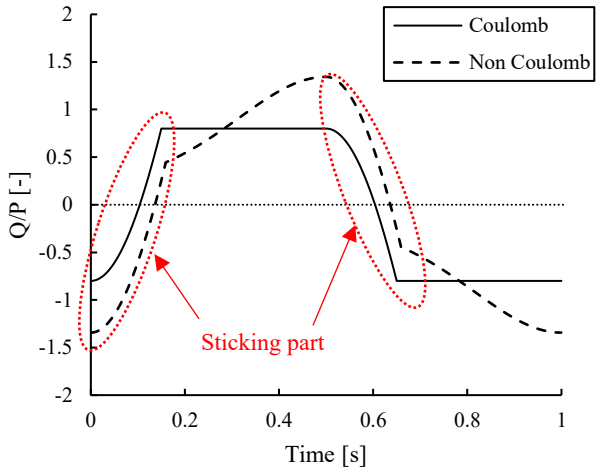

Fig. 3. Evolution of the CoF within a fretting cycle.

Logically, due to the influence of the system stiffness in the fretting loop, only the sliding portion needs to be taken into account in computing the mean value. This approach, however, requires introducing cumbersome algorithms in order to detect the sliding part of the cycle, as the slip amplitude may not remain constant throughout the test. A simpler alternative was recently applied by Wang et al. [20], who averaged the tangential force in a window between Q_{max} and $0.8 \cdot Q_{max}$. In the non-Coulomb condition, however, this method overestimates the actual CoF (similar to max(CoF) method), as only the near-peak values are considered.

2.3 Energy coefficient of friction

Due to the issues experienced in applying the above-mentioned methods in the presence of hook-like features across the fretting loop, Fouvry et al. [21] developed the ECoF method and explained the non-Coulomb behaviour of the tangential force by the physical interaction between the edges of the wear scar. The authors attributed this effect to the material accumulation in the contact edges due to the plastic flow of the material (see Fig. 15 in ref [21]). To minimise this effect of wear scars interaction, Fouvry et al. proposed a method—which was also used at the time by Klaffke [22]—based on the energy dissipation over the fretting loop to calculate the CoF, the so-called ECoF. This method was formulated as:

$$\mu_E = \frac{E_d}{4P\delta^*}, \tag{1}$$

where E_d is the dissipated energy over a cycle, δ^* is the slip amplitude and P is the contact load. The simplicity and the robustness of the method popularised it in the field, and it later evolved into an

American Society for Testing and Materials or ASTM standard [23]. The ECoF seeks to find a representative CoF of the cycle and is therefore dependent on the stroke and stiffness of the contact system [22, 24].

2.4 Geometric independent coefficient of friction

As previously mentioned, the increase in the frictional force across the stroke is a commonly observed phenomenon in fretting. Mulvihill et al. [24] demonstrated with a simple mechanical model that the hook-like behaviour results from the interaction of the normal force (F_N) and friction force (F_R) across the groove shape. As shown in **Fig. 4**, both F_N and F_R (μF_N) forces contribute to the tangential load (Q) and contact load (P) due to the contact axes rotation generated by the wear scar geometry. The wear scar shape was assumed to be parabolic:

$$z = z_0 \left(\frac{x}{x_0} \right)^2, \tag{2}$$

where z_0 is the depth, x_0 is the half-width of the groove, and x is the position at each point in the x axis, where z_0 and x_0 are set to be the maximum displacement normal to the reciprocating movement and to be equal to the applied displacement amplitude (Δ^*), respectively. Accordingly, Mulvihill's model successfully predicted the increase of the tangential force Q in gross sliding regime for deeper and/or lower width groove.

Jin et al. [11] further advanced the mechanical model developed by Mulvihill et al. In order to simulate the stiffness of the contact system, the former rigid model (Mulvihill et al. model) was modified by introducing a spring (**Fig. 4 (a)**). Thus, the relation between the real slip (δ) and the applied displacement (Δ) could be successfully predicted as:

$$\delta = \Delta - \frac{Q}{S}, \tag{3}$$

$$Q = P \cdot \frac{\mu \cdot \frac{|\dot{\delta}|}{\dot{\delta}} + \left(\frac{2z_0}{x_0^2} \cdot x \right)}{1 - \mu \cdot \frac{|\dot{\delta}|}{\dot{\delta}} \cdot \left(\frac{2z_0}{x_0^2} \cdot x \right)}, \tag{4}$$

where μ is the true contact CoF, $|\dot{\delta}|/\dot{\delta}$ is the direction of motion of the indenter in the sliding portion, z_0 is the depth, x_0 is the half-width of the groove, and x is the position at each point on the x axis.

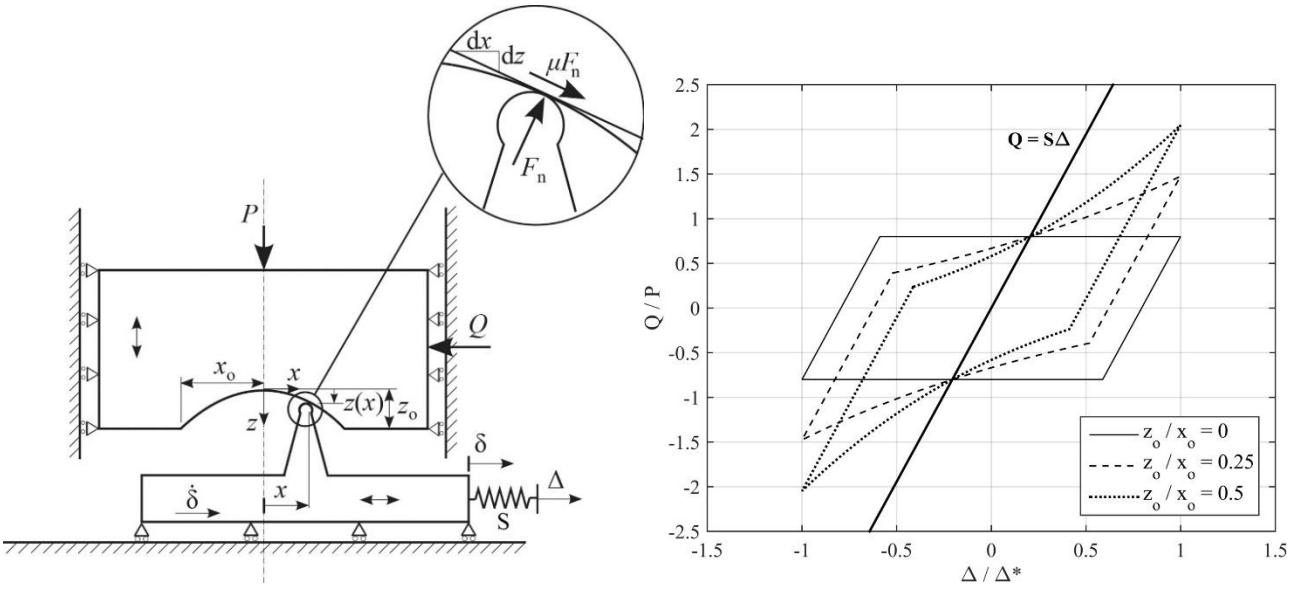

(a) (b)

Fig. 4. (a) Illustration of wear-scar interaction model with inclusion of the stiffness of the rig (based on Mulvihill et al.'s model by [24]); (b) Comparison of fretting loops with grooves of different aspect ratios (Reproduced with permission of Elsevier) [11].

Additionally, they proposed to derive the true contact CoF (μ, which they termed GICoF) at the point where the slope of the wear groove shape is zero (i.e. the friction force and the tangential force vectors are parallel, thus $\mu = Q/P$). **Fig. 4 (b)** shows the obtained fretting loops for different groove depths (z_0) while all other parameters are constant. All hysteresis loops intersect at two points, which is the actual centre of the wear scar. Therefore, in order to compute the GICoF, it suffices to find the point where the hysteresis loop intersects with the function $Q = S\Delta$, i.e. the function with a slope equal to the system stiffness *S* that crosses the origin. This method assumes that the CoF is constant throughout the stroke and its variation is only due to geometrical effects in the measurement. A similar approach was employed by Diomidis et al. [25, 26] where the CoF was computed by taking the tangential force when the indenter was in the middle of the stroke.

However, the method has a drawback that it only uses one point to compute the CoF. It could, therefore, be very sensitive to noise and appropriate filtering may be necessary. On the other hand,

the concept behind the method is relatively new and it needs to be explored whether it is applicable under different circumstances.

3. Synthetic data analysis

In this section the impact of the derivative method according to the fretting loop shape is analysed via virtually generated synthetic fretting loop theoretical analysis. Four simulated FLs with different characteristics were generated following Jin et al.'s model [11] (Eq. 2–3), i.e. those loops were modelled as a one-point interaction between two rigid bodies (**Fig. 4**). The following sections describe, first, the details of the loops developed (section 3.1), followed by the description of the results obtained and the respective discussion (section 3.2).

3.1 Synthetic fretting loops

To analyse the accuracy of each method in deriving the coefficient of friction under gross sliding condition, typical fretting loops were virtually generated with a known imposed CoF value following Jin et al.'s model [11]. This model accounts for the stiffness of the contact system (*S*), the real slip (δ), the applied displacement (Δ^*) and the true contact CoF (μ), including the geometry of the wear scar by means of the depth (z_0) and the half-width of the groove (x_0). The algorithm employed in generating the described fretting loops is described in Appendix A.

Four fretting loops—depicted in **Fig. 5** and described below—were generated following the parameters listed in **Table 1**. All models correspond to an imposed CoF of 0.8—which represents the target value in the study in order to account for the accuracy of the derivation methods—, a sinusoidal displacement and an acquisition frequency of 2kHz per cycle. Additionally, some of the same parameters were applied on all loops, namely, the contact force *P* (450 N), the applied displacement amplitude Δ^* (50 μm) and the half-width of the wear scar x_0 (50 μm).

The first fretting loop (FL1) corresponds to an idealised fretting loop with no wear scar in Coulomb friction conditions [27]. The remaining loops (FL2-4) represent idealizations of different non-Coulomb frictional behaviour, at which the tractional force increases during the whole gross sliding stage reaching the maximum at the end of the stroke [24, 28]. FL2 and FL3 correspond to fretting loops with the same wear scar (10 μm depth) but different system stiffness (100000 and 20000 N/mm respectively), which generates differently distorted fretting loops. Finally, FL4 represents both higher stiffness than FL3 (60000 N/mm) and deeper wear scar (50 μm) providing a pronounced non-

Coulomb behaviour in the loop shape. Based on the mass review presented in section 2, it can be concluded that FL1 and FL2 are the most typical loops described in literature.

Table 1. Summary of the parameters for generating the four fretting loops (FLs).

Variables	**Unit**	FL1	FL2	FL3	FL4
P	N	450	450	450	450
S	N/mm	100000	100000	20000	60000
x_0	μm	50	50	50	50
z_0	μm	0	10	10	25
Δ^*	μm	50	50	50	50
μ	-	0.8	0.8	0.8	0.8

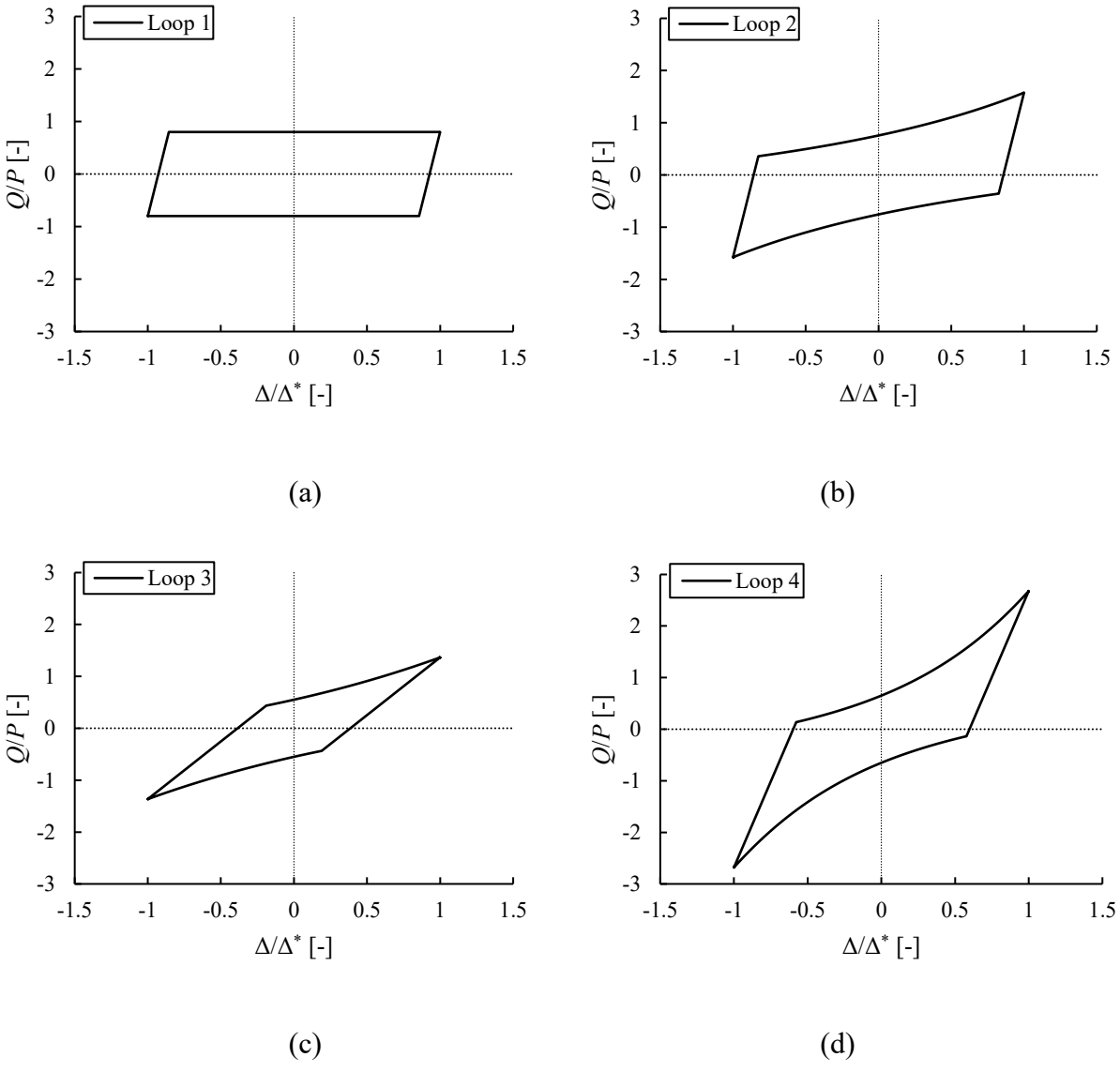

Fig. 5. Simulated fretting loops: (a) FL1; (b) FL2; (c) FL3; (d) FL4.

3.2 Results and discussion

Fig. 6 depicts the results obtained with the four CoF derivation methods under study: max(CoF), mean(CoF), ECoF, GICoF, at each of the four virtually generated fretting loops (FL1–FL4).

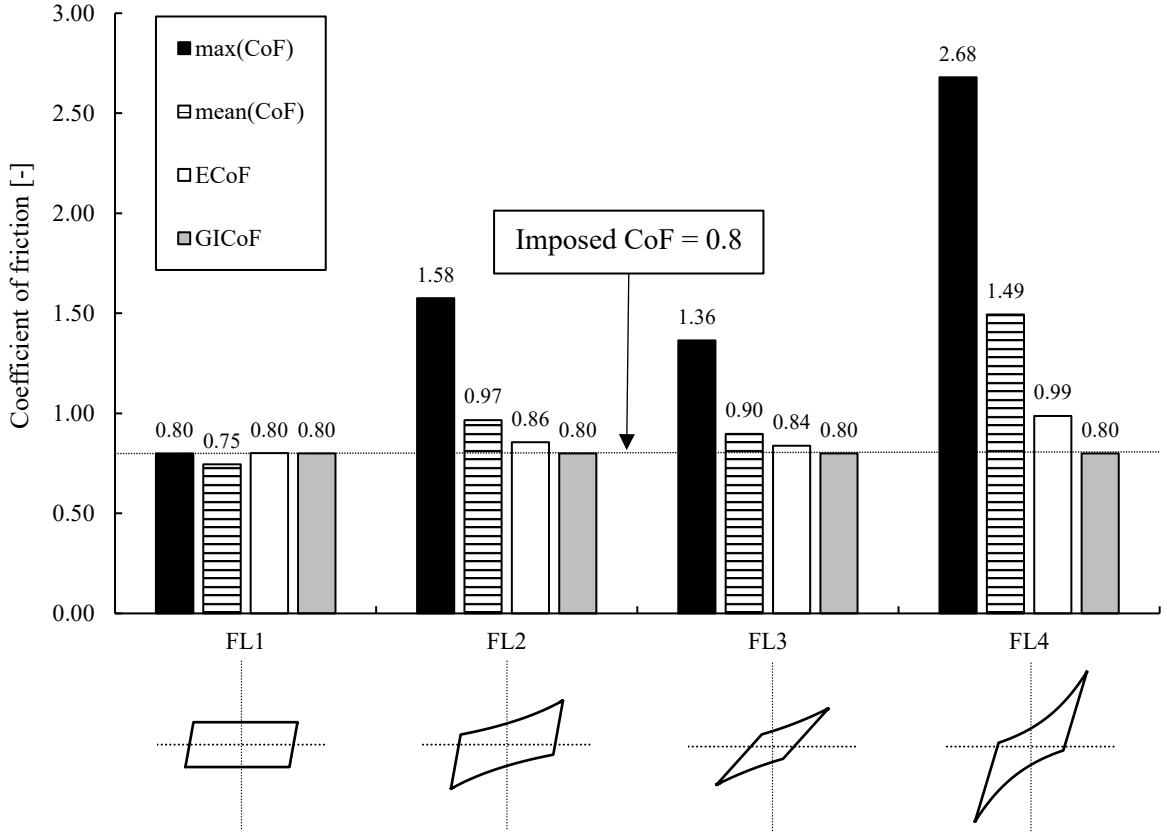

Fig. 6. Simulated fretting loop results according to the considered CoF methods.

As can be observed, only the GICoF method reported the targeted true contact CoF value for all fretting loops under study. This was expected since this method is affected neither by groove geometry nor by system stiffness. The remaining methods resulted in errors of different magnitudes. This finding underlines the limitations of the methods and allows to assess the sensitivity under different casuistic.

As can be observed, the max(CoF) produced an accurate result only in the Coulomb behaviour fretting loop (FL1). The errors obtained are dependent on the distortion of the loop, providing errors for FL2, FL3 and FL4 of 97%, 70%, and 235%, respectively, which demonstrates its weakness to report the true contact friction coefficient.

The mean(CoF) method reported deviations from the target value in all cases under study. With FL1, this deviation is caused by the sticking part, which slightly reduced the mean(CoF) as discussed in section 2. In the remaining cases, this method yields larger error values, the largest one for FL4 with an error of 87%. It is noteworthy that, when computing the mean value, the quantity of the data points along the fretting loop is not equal during the gross sliding distance, since the acquisition frequency is constant but the velocity varies. **Fig. 7** shows the distribution of the tangential force numerical data divided in ranges of 0.2 N. Multiple data points are located near the $Q_{\max}$ location due to the low velocity at the end of the stroke, which increases the contribution of higher tractional forces in the mean value and leads to an increase in the computed CoF value.

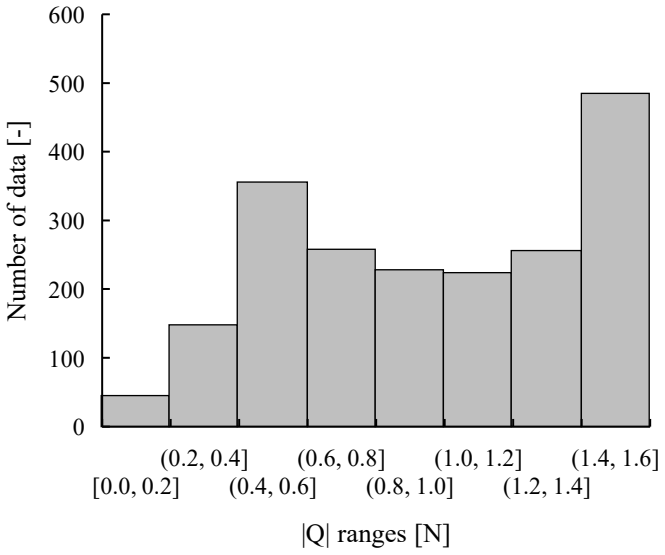

Fig. 7. Histogram of the fretting loop data points.

The ECoF method generally produced higher CoF values than the target, but proved to be reasonably accurate within the usual scatter of tribological tests. However, the method's primary dependency on the groove geometry can be observed in the case exhibiting the most extreme non-Coulomb behaviour, namely, FL4, at which the obtained error was 23%. It can be concluded that the method yields reasonable values when the wear scar remains shallow.

In general, it is observed that the fretting loops exhibiting non-Coulomb behaviour requires to select carefully the CoF derivation method in order to obtain an accurate friction coefficient value. It was proven that both max(CoF) and mean(CoF) methods report large overestimations of the coefficient of friction and are, therefore, not suitable for gross sliding fretting analysis. According to the mass literature review, these methods continue to be widely applied, with as many as 37% of the published

papers computing the CoF by using max(CoF) and mean(CoF) methods. For all that, it is worth stressing that 41% of the papers did not specify their derivation method, which begs the question whether the reported data are indeed overestimated.

4. Experimental data analysis

In this section, the four methods under analysis were tested with combined fretting wear and fretting fatigue experiments. A crossed cylinder contact configuration was used in order to experimentally generate different fretting loop shapes. This contact configuration allows to change the crossing angle between wires (cylinders) under the same material and obtain different wear scar geometries as we demonstrated in earlier studies [19, 29]. For higher crossing angles, a decrease of the wear scar width and an increase of the groove depth were observed (**Fig. 8**).

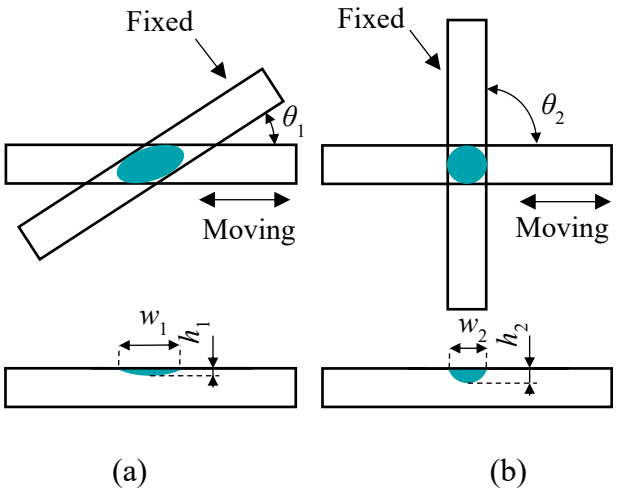

Fig. 8. Crossed cylinder contact configuration sketches. In the top row the top view of the contact is shown. In the bottom row the side view of the wear scar is shown: (a) crossing angle of θ_1; (b) crossing angle of θ_2.

4. 1 Fretting test apparatus

The self-made test apparatus employed in these tests (**Fig. 9**) is briefly described in the following paragraph (for a detailed description of the tribostester see [19]). The modular design of the tribometer allows performing fretting wear, fretting fatigue or combined fretting wear and fretting fatigue tests depending on the selected configuration. An electric motor converts the rotational movement into highly stable reciprocating stroke, which is able to control reciprocated displacements raging between 10 and 5000 μm. In fretting fatigue configuration, the actual displacement at the contact point is generated by straining the fatigued wire. On the other hand, the contact load is applied with a screw

connected to a spring, which allows for applying the contact load within the 0.1–10N range. The tangential load is generated due to the displacement between the fatigued wire and contacting wires.

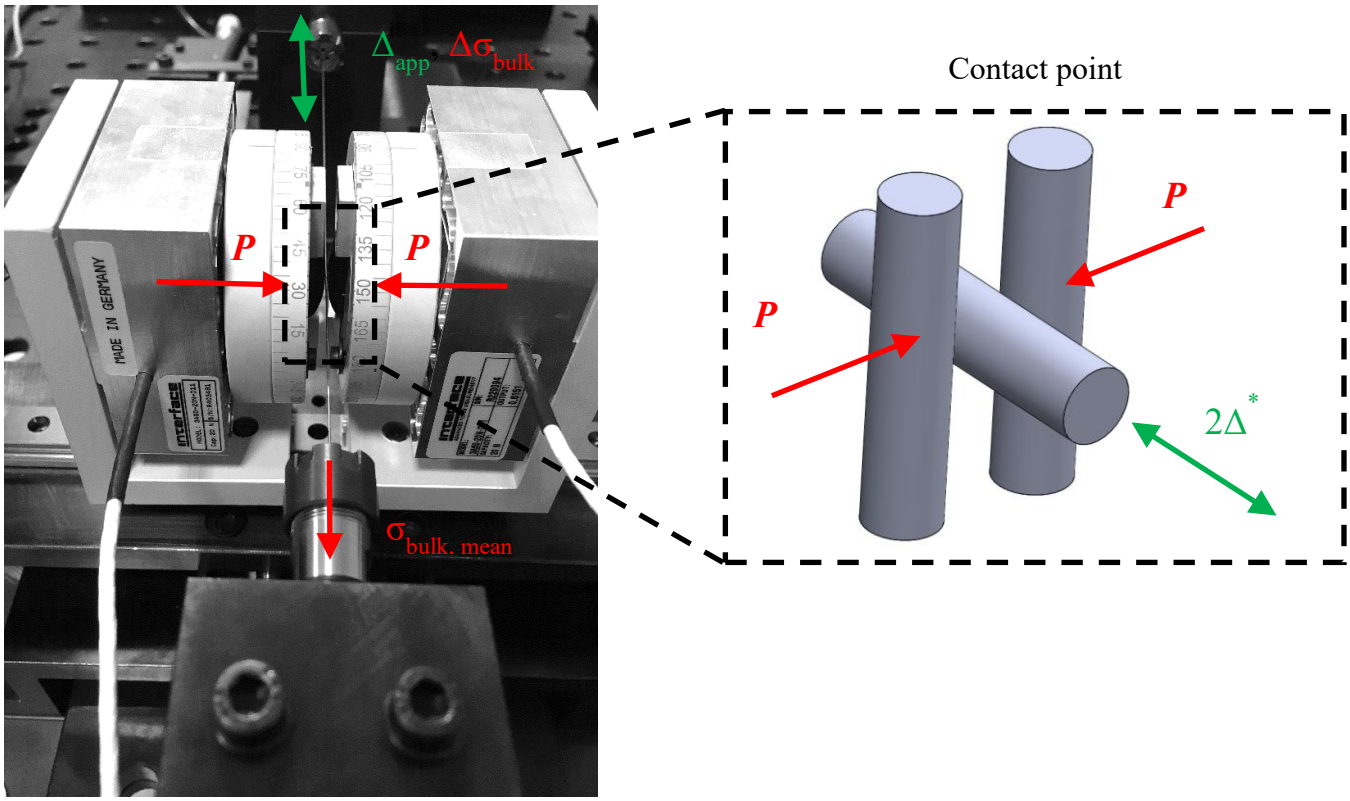

Fig. 9. Detail of the self-made tribotester with the contact module for fretting fatigue configuration.

4. 2 Test parameters selection

Cold drawn eutectoid carbon steel (0.8% C) wire of 0.45 mm diameter typically used in the lift industry (7 × 19 stranded rope) was employed. In our earlier study [30], plastic deformation at the contact points was found in a newly assembled rope. A simple Hertzian pressure analysis disclosed that contact forces in the range of 1–5 N (depending on the contact angle) can result in plastic deformation. Accordingly, a contact load of 2 N was selected as a representative contact force. Additionally, longitudinal abrasive scars were detected in the range from 60 to 100 μm. We previously identified representative strokes of 65 and 130 μm [29–31]. In the present study, a displacement amplitude of 100 μm was consequently selected. It should be mentioned that in the initial stage of the test, reciprocating sliding (instead of fretting) was detected following the definition provided in [32]. However, owing to the rapid increase of the contact area in crossed cylinder contact configuration due to wear, a transition to fretting regime was ensured in all cases. It should be noted

that all tests were stopped before the fracture of the wire. Three repetitions were performed for each test configuration. Considering two different contact at each side of the fatigued wire, virtually six different tests were carried out for each test condition. Finally, a summary of the tests conditions and material properties are presented in **Table 2** and **Table 3**, respectively.

Table 2. Fretting tribological test conditions.

Properties	Symbol	Unit	Value	Tribosystem
Contact load	P	N	2	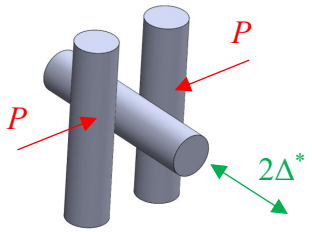
Crossing angle	α	°	0;45;90	
Average contact pressure	p_{av}	MPa	--;2615;3100	
Maximum Hertz pressure	p_{max}	MPa	--;3472;4650	
Maximum bulk stress	$\sigma_{k,max}$	MPa	880	
Minimum bulk stress	$\sigma_{k,min}$	MPa	314	
Tangential stress ratio	R_Q	-	-1	
Stroke	$2\Delta^*$	µm	100	
Frequency	υ	Hz	3	
Number of cycles (10^3)	N	-	150	
Lubricant		-	None	
Temperature	T	°C	22±2	
Atmosphere		-	Laboratory air	
Relative humidity	RH	%	50±5	

Table 3. Geometrical, mechanical and surface properties.

Properties	Symbol	Unit	Value
Fatigued wire length	L	mm	155
Wire diameter	d	mm	0.45
Tensile strength	σ_u	MPa	>3200
Yield strength	σ_y	MPa	>2650
Elastic modulus	E	GPa	200
Vickers hardness	HV0.05	-	659±81
Average roughness drawn direction (DD)	R_a	µm	0.35
Average roughness perpendicular to the DD	R_a	µm	0.7

4.3. Results and discussion

A non-contact 3D optical profiler (Sensofar S-Neox, white light interferometry technique) was used with an objective of 20xDI (optical resolution = 0.41 µm, vertical resolution 1 nm) in order to measure the wear scars. Following the 3D areal measurements (2450x267 µm area), 2D profiles were extracted to characterise the wear scar width and depth in SensoMap Premium 7 software. **Fig. 10** shows the

wear scars obtained at the end of the test ($150 \cdot 10^3$ cycles) for fixed contacting wires. Shorter width and higher wear depth are obtained for higher crossing angles.

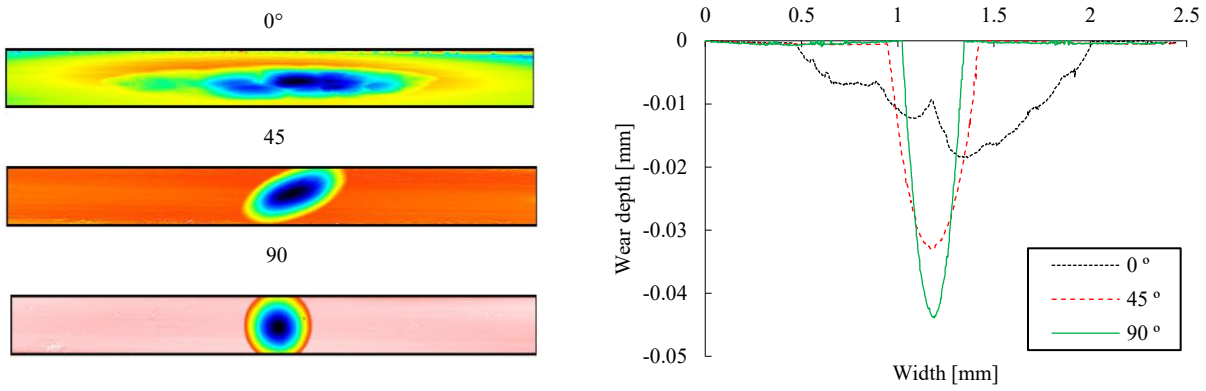

(a) (b)

Fig. 10. Representative wear scars: (a) 3D view of the wear scar for 0º, 45º and 90º crossing angle (free scale); (b) 2D profile of the wear scar parallel to the wire axis (imposed scale).

Fig. 11 shows the evolution of the friction coefficient during the test calculated by applying the analysed methods (**Fig. 11 (a,c,e)**, left column) along with the fretting loops (**Fig. 10 (b,d,e)**, right column) for the three crossing angles presented. **Fig. 11(a)** demonstrates that the mean(CoF), the ECoF, and the GICoF show very similar trends for the 0° cross angle test. On the other hand, the max(CoF) produced an approximately 25% higher value than the other methods. The latter was unexpected since the fretting loops were close to the flat-topped shape during the entire test (**Fig. 11(b)**), similar to the FL1 of the previous section. It should be mentioned, however, that the max(CoF) method is very sensitive to small variation, and, in this analysis, it failed to capture accurately the CoF even in nearly flat toped conditions. This analysis brings into question whether the reported CoFs using the max(CoF) are overestimated values even in flat-toped conditions, which is potentially quite consequential since this is the most commonly used method.

In the case of 45° crossing angle test a clear difference between the four methods was observed (**Fig. 11(c)**). These differences were expected since the FLs demonstrated non-Coulomb behaviour (**Fig. 11(d)**). Similar to the synthetic FL data analysis, the highest CoF was calculated by the max(CoF) method followed by the mean(CoF). The differences between the ECoF and the GICoF (**Fig. 11(c)**) steadily increased for higher number of cycles (up to 10~15% difference) due to a more pronounced non-Coulomb behaviour occurring in the final stage of the test. It should be highlighted that the theoretical model analysed in the previous section (i.e. the one-point interaction between two rigid

bodies model) cannot be applied in this case as both contacting wires wear out heavily, whereas the analytical model only considers a single-groove pad.

The 90° test showed similar trends to the 45° test, although higher differences were obtained (**Fig. 11(e) and Fig. 11(f)**). Both the max(CoF) and the mean(CoF) showed their inability to capture accurately the actual CoF. The GICoF showed almost a constant value throughout the entire test whereas a steady increase of the ECoF value was observed during the test without reaching a stable value. In the case of the GICoF, it was observed that almost all fretting loops intersected at two points (**Fig. 11(f)**), which were the GICoF measurement points (cf. section 2.4). The two methods (GICoF and ECoF) exhibited a 36% difference for the 90° test, which was considerably higher the maximum reported difference of 13% observed in [11].

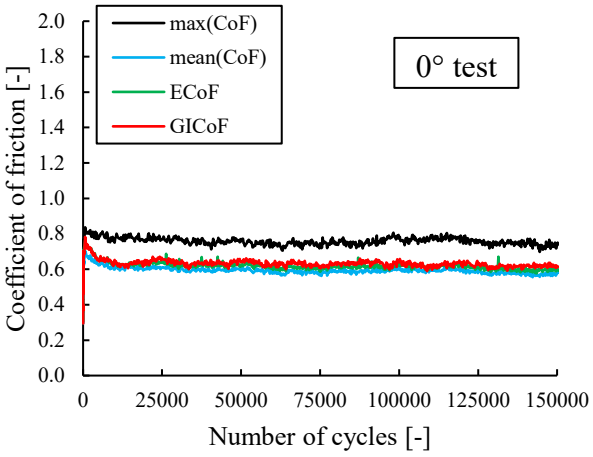

(a)

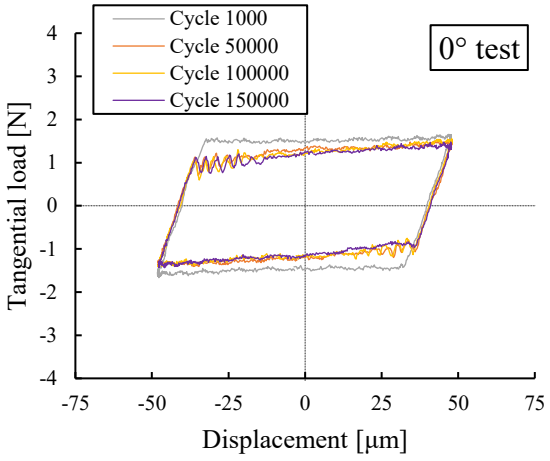

(b)

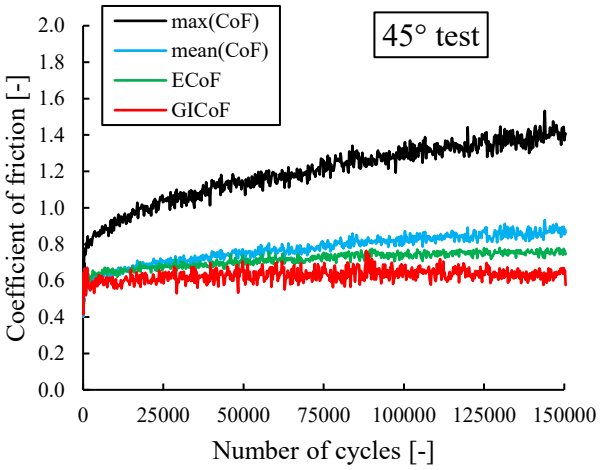

(c)

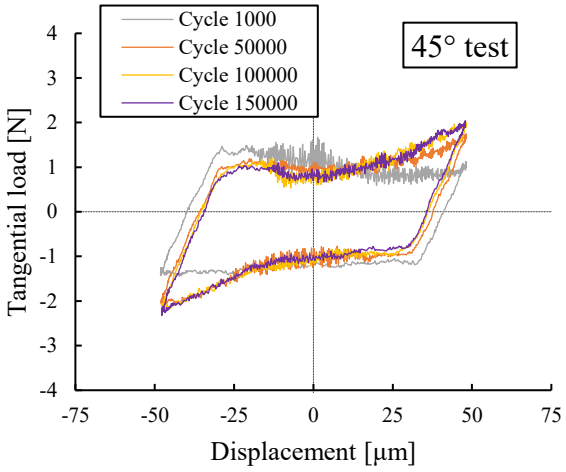

(d)

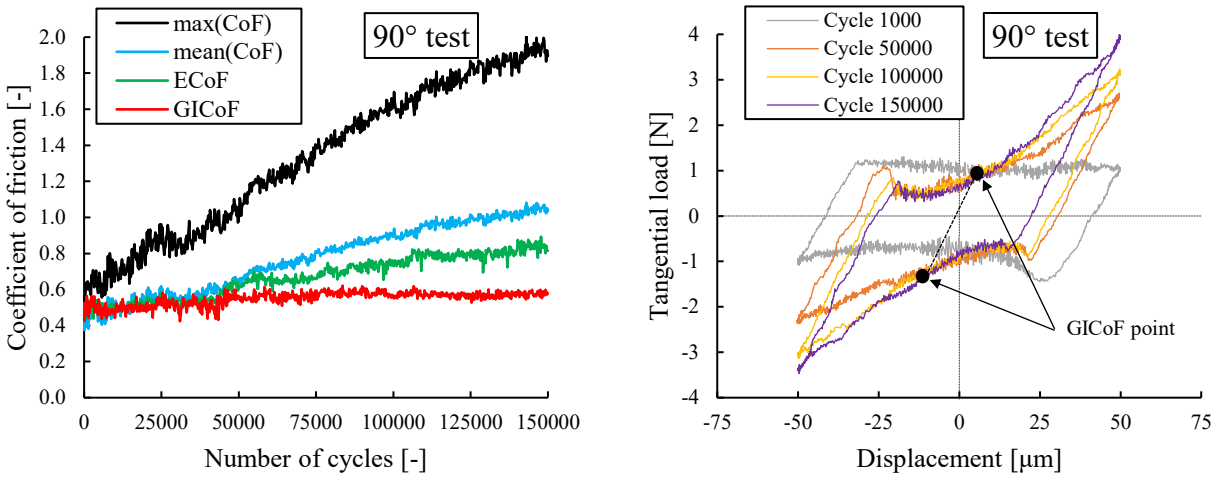

(e) (f)

Fig. 11. Comparison of the evolution of the max(CoF), mean(CoF), ECoF and GICoF (left column) along with the developed fretting loops at different stages (right column) for the three crossing angles presented: (a) and (b) 0º; (c) and (d) 45º; (e) and (f) 90º.

Mean values and standard deviations of the CoF value evolutions depicted in **Fig. 11** are summarised in **Fig. 12**. As previously mentioned, overall both max(CoF) and mean(CoF) methods reported the highest values in all analysed cases, which according to the previous theoretical study, could be associated with overestimations of the true contact coefficient of friction. As for the ECoF and GICoF methods, both computed the same values for the 0º cross angle case. This result is expected, since this case does not present an important wear scar, and, therefore, does not exhibit non-Coloumb behaviour, which could distort the values of the ECoF, as discussed in the theoretical analysis. Accordingly, the value of the ECoF for the cross angles of 45º and 90º increases, due to the increasing non-Coloumb behaviour of the fretting loop shape associated with the wear scar. The GICoF produces the most robust values. Although there is a slight decrease in the 90º angle, considering the typical deviation in tribological tests, the CoF arguably does not significantly change with the crossing angle. The GICoF method is thus the most appropriate derivative method for gross sliding conditions.

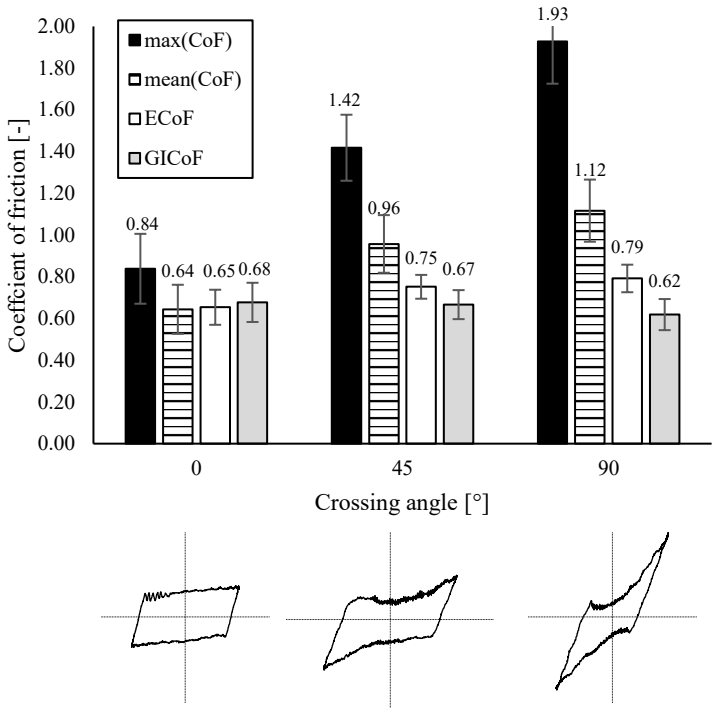

Fig. 12. Obtained CoF values and the standard deviation for different crossing angles (top row). Representative images of the fretting loop shapes corresponding to cycle 150000 (bottom row).

To summarise, the coefficient derivation method greatly influenced the obtained results both in the synthetic and in the case study. The case study disclosed differences that were not identified in the theoretical study due to the noise and characteristics of real test signals. In the former case, the max(CoF) method represented deviations even in the nearly flat topped shaped loops due to the sensitivity to outlier points. The results obtained through the studied derivation methods differed up to 211%, which highlights the importance of the appropriate method selection in reporting accurate data for characterising and simulating the tribosystem. In spite of the importance of the selected method, the mass literature review showed that 41% of studies published in top tribological journals do not mention their selected method, and 37% used the mean(CoF) and the max(CoF) methods, both of which potentially greatly overestimate the CoF in gross sliding conditions. Progress in fretting science depends on rigorous and effective communication; therefore, clearly specifying the coefficient derivative method and reporting the fretting loop shape is essential. The use of the GICoF method is suggested for gross sliding regime analysis. Seeing, however, that this is a relatively new method, it lends itself to further casuistic studies in order to determine its robustness.

5- Conclusions

This study set out to conduct a critical analysis of coefficient of friction derivation methods for fretting under gross slip regime. The following conclusions were drawn from the obtained results:

- The GICoF proved to be the most robust method considering both the analytical and experimental analysis. Its use is suggested for practice, although, seeing that it is a relatively new method, it arguably lends itself to further casuistic studies in order to determine its robustness.
- The ECoF disclosed higher CoF values than the GICoF for loops exhibiting highly pronounced non-Coloumb behaviour, but a reasonably good accuracy within the usual scatter of tribological tests was obtained. However, the primary dependency of the method on the groove geometry was observed in the case exhibiting the most extreme non-Coulomb behaviour.
- Both the max(CoF) and the mean(CoF) methods reported great overestimations of the coefficient of friction in non-Coulomb fretting loops, and, therefore, they are not suitable for non-Coulomb gross sliding fretting cases. Additionally, the max(CoF) showed deviations even in the nearly flat topped shaped loops.
- The mass literature review revealed that 37% of the published studies calculated the CoF using max(CoF) and mean(CoF) methods, and 41% failed to specify the derivation method used. This calls into question whether the reported data are overestimated or not.
- Progress in fretting science depends on rigorous and effective communication; therefore, clearly specifying the coefficient derivative method and reporting the fretting loop shape is essential for research with archival value.

Appendix A: Employed algorithm to generate the synthetic fretting loops.

1. First, a sinusoidal signal vector of equal length to the frequency acquisition time was generated.
2. The generated vector was multiplied with the applied displacement amplitude Δ^* to determine all displacement points.
3. $\pm Q$ vectors were calculated using Eq. 4. The influence of the system stiffness was not considered at this stage.
4. In order to consider the system stiffness, Eq. 3 was introduced in Eq. 4 where $x = \delta$. The following equation was obtained:

$$Q = P \cdot \frac{\mu \cdot \frac{|\dot{\delta}|}{\dot{\delta}} + \left(\frac{2z_0}{x_0^2} \cdot \left(\Delta - \frac{Q}{S} \right) \right)}{1 - \mu \cdot \frac{|\dot{\delta}|}{\dot{\delta}} \cdot \left(\frac{2z_0}{x_0^2} \cdot \left(\Delta - \frac{Q}{S} \right) \right)} \tag{5}$$

5. The variable Q is at both sides of the equation. Therefore, Eq. 5 was solved iteratively, using the previously calculated $\pm Q$ vectors as initial values.
6. Two lines were generated $Q = S \cdot \Delta \pm \Delta^*$ in order to consider the micro-slip part of the fretting loop, and the intersecting points were calculated between these vectors and the previously one calculated in the fifth step.
7. The final Q vector was updated to consider the micro-slip parts.

Acknowledgments

The authors gratefully acknowledge the financial support given by the Eusko Jaurlaritza under "Programa de apoyo a la investigación colaborativa en áreas estratégicas" (Project MEDECA: Ref. KK-2017/00053, and MEDECA2: Ref. KK-2018/00013) programs.

References

[1] Waterhouse RB. Fretting wear. Wear 1984;100:107–18. doi:10.1016/0043-1648(84)90008-5.
[2] Waterhouse RB, Taylor DE. Fretting debris and the delamination theory of wear. Wear 1974;29:337–44. doi:10.1016/0043-1648(74)90019-2.
[3] Hills DA, Nowell D. Mechanics of Fretting Fatigue. Springer; 1994.
[4] Anandavel K, Prakash RV. Effect of three-dimensional loading on macroscopic fretting aspects of an aero-engine blade–disc dovetail interface. Tribol Int 2011;44:1544–55. doi:10.1016/j.triboint.2010.10.014.
[5] Kim H-K, Lee Y-H, Heo S-P. Mechanical and experimental investigation on nuclear fuel fretting. Tribol Int 2006;39:1305–19. doi:10.1016/j.triboint.2006.02.027.
[6] Cruzado A, Leen SB, Urchegui MA, Gómez X. Finite element simulation of fretting wear and fatigue in thin steel wires. Int J Fatigue 2013;55:7–21. doi:10.1016/j.ijfatigue.2013.04.025.
[7] Kim K, Geringer J, Pellier J, Macdonald DD. Fretting corrosion damage of total hip prosthesis: Friction coefficient and damage rate constant approach. Tribol Int 2013;60:10–8. doi:10.1016/j.triboint.2012.10.008.
[8] Zeng D, Zhang Y, Lu L, Zou L, Zhu S. Fretting wear and fatigue in press-fitted railway axle: A simulation study of the influence of stress relief groove. Int J Fatigue 2019;118:225–36. doi:10.1016/j.ijfatigue.2018.09.008.
[9] Dobromirski JM. Variables of Fretting Process: Are There 50 of Them? Stand Fretting Fatigue Test Methods Equip 1992. doi:10.1520/STP25816S.

[10] Dobromirski J, Smith IO. A stress analysis of a shaft with a press-fitted hub subjected to cyclic axial loading. Int J Mech Sci 1986;28:41–52. doi:10.1016/0020-7403(86)90006-8.
[11] Jin X, Sun W, Shipway PH. Derivation of a wear scar geometry-independent coefficient of friction from fretting loops exhibiting non-Coulomb frictional behaviour. Tribol Int 2016;102:561–8. doi:10.1016/j.triboint.2016.06.012.
[12] Kim K, Korsunsky AM. Dissipated energy and fretting damage in CoCrAlY-MoS2 coatings. Tribol Int 2010;43:676–84. doi:10.1016/j.triboint.2009.10.007.
[13] Hintikka J, Lehtovaara A, Mäntylä A. Fretting-induced friction and wear in large flat-on-flat contact with quenched and tempered steel. Tribol Int 2015;92:191–202. doi:10.1016/j.triboint.2015.06.008.
[14] Magaziner R, Jin O, Mall S. Slip regime explanation of observed size effects in fretting. Wear 2004;257:190–7. doi:10.1016/j.wear.2003.12.005.
[15] Lee H, Mall S. Fretting behavior of shot peened Ti–6Al–4V under slip controlled mode. Wear 2006;260:642–51. doi:10.1016/j.wear.2005.03.022.
[16] Everitt NM, Ding J, Bandak G, Shipway PH, Leen SB, Williams EJ. Characterisation of fretting-induced wear debris for Ti-6Al-4 V. Wear 2009;267:283–91. doi:10.1016/j.wear.2008.12.032.
[17] Fouvry S, Kapsa P, Zahouani H, Vincent L. Wear analysis in fretting of hard coatings through a dissipated energy concept. Wear 1997;203–204:393–403. doi:10.1016/S0043-1648(96)07436-4.
[18] Paulin C, Fouvry S, Meunier C. Finite element modelling of fretting wear surface evolution: Application to a Ti–6A1–4V contact. Wear 2008;264:26–36. doi:10.1016/j.wear.2007.01.037.
[19] Llavori I, Zabala A, Otaño N, Tato W, Gómez X. Development of a Modular Fretting Wear and Fretting Fatigue Tribometer for Thin Steel Wires: Design Concept and Preliminary Analysis of the Effect of Crossing Angle on Tangential Force. Metals 2019;9:674. doi:10.3390/met9060674.
[20] Wang D, Song D, Wang X, Zhang D, Zhang C, Wang D, et al. Tribo-fatigue behaviors of steel wires under coupled tension-torsion in different environmental media. Wear 2019;420–421:38–53. doi:10.1016/j.wear.2018.12.038.
[21] Fouvry S, Duó P, Perruchaut Ph. A quantitative approach of Ti–6Al–4V fretting damage: friction, wear and crack nucleation. Wear 2004;257:916–29. doi:10.1016/j.wear.2004.05.011.
[22] Klaffke D. Towards a tribological reference test - fretting test ? Int Coll Tribol., vol. 3, TAE Esslingen; 2004, p. 1839–46.
[23] G02 Committee. Guide for Determining Friction Energy Dissipation in Reciprocating Tribosystems. ASTM International; n.d. doi:10.1520/G0203-10R16.
[24] Mulvihill DM, Kartal ME, Olver AV, Nowell D, Hills DA. Investigation of non-Coulomb friction behaviour in reciprocating sliding. Wear 2011;271:802–16. doi:10.1016/j.wear.2011.03.014.
[25] Diomidis N, Mischler S, More NS, Roy M, Paul SN. Fretting-corrosion behavior of β titanium alloys in simulated synovial fluid. Wear 2011;271:1093–102. doi:10.1016/j.wear.2011.05.010.
[26] Diomidis N, Mischler S. Third body effects on friction and wear during fretting of steel contacts. Tribol Int 2011;44:1452–60. doi:10.1016/j.triboint.2011.02.013.
[27] Coulomb CA. Théorie des machines simples en ayant égard au frottement de leurs parties et à la roideur des ... Bachelier; 1821.
[28] Hintikka J, Lehtovaara A, Mäntylä A. Normal displacements in non-Coulomb friction conditions during fretting. Tribol Int 2016;94:633–9. doi:10.1016/j.triboint.2015.10.029.
[29] Cruzado A, Hartelt M, Wäsche R, Urchegui MA, Gómez X. Fretting wear of thin steel wires. Part 2: Influence of crossing angle. Wear 2011;273:60–9. doi:10.1016/j.wear.2011.04.012.
[30] Urchegui MA, Hartelt M, Klaffke D, Gómez X. Laboratory fretting tests with thin wire specimens. Tribotest 2007;13:67–81. doi:10.1002/tt.34.

[31] Cruzado A, Hartelt M, Wäsche R, Urchegui MA, Gómez X. Fretting wear of thin steel wires. Part 1: Influence of contact pressure. Wear 2010;268:1409–16. doi:10.1016/j.wear.2010.02.017.
[32] Fouvry S. Etude quantitative des dégradations en fretting. PhD Thesis. 1997.